Magnetically ordered Cu and Ru in $Ba_2GdRu_{1-u}Cu_uO_6$ and in $Sr_2YRu_{1-u}Cu_uO_6$

Howard A. Blackstead
Department of Physics, University of Notre Dame, Notre Dame, Indiana 46556

John D. Dow
Department of Physics, Arizona State University, Tempe, Arizona 85287-1504

Dale R. Harshman
*Physikon Research Corporation, P. O. Box 1014, Lynden, Washington 98264;**
Physics Department, University of Notre Dame, Notre Dame, Indiana 46556;
and Physics Department, Arizona State University, Tempe, Arizona 85287-1504

W. B. Yelon and Ming Xing Chen
University of Missouri, Research Reactor Facility, Research Park, Columbia, Missouri 65211

M. K. Wu and D. Y. Chen†
Department of Physics and Materials Science Center, National Tsing Hua University, Hsinchu, Taiwan

F. Z. Chien
Physics Department, Tamkang University, Tamsui, Taiwan

D. B. Pulling
Department of Physics, University of Notre Dame, Notre Dame, Indiana 46556
(Received 13 June 2000; revised manuscript received 16 August 2000; published 9 May 2001)

Magnetic orderings of the Cu, Gd, and Ru moments in nonsuperconducting $Ba_2GdRu_{1-u}Cu_uO_6$ and of the Cu and Ru moments in superconducting $Sr_2YRu_{1-u}Cu_uO_6$ (whose superconducting onset temperature is ~45 K) have been studied using dc susceptibility, microwave magnetic resonance, and neutron diffraction (on $Sr_2YRu_{0.85}Cu_{0.15}O_6$ only). In both homologues, Cu exhibits antiferromagnetism with an ordering temperature of ~86 K (much greater than the resistive superconductivity onset transition of ~45 K), and a magnon energy gap $\hbar\omega_{\text{magnon}}$ $(q=0)$ that exceeds the microwave photon frequency of $\omega/2\pi=13$ GHz. The Cu moment extracted from neutron data for $Sr_2YRu_{1-u}Cu_uO_6$ is $\sim 1.7\mu_B$ at low temperature. Gd, in $Ba_2GdRu_{1-u}Cu_uO_6$, is paramagnetic and displays a $g=2$ electron spin resonance at temperatures above ~48 K, which also persists well below ~48 K (but with a very much broadened line), and orders antiferromagnetically at ~12 K. Ru in $Ba_2GdRu_{1-u}Cu_uO_6$ orders at ~48 K, but in $Sr_2YRu_{1-u}Cu_uO_6$ orders at ~23 K and has a moment of $\sim 1.6\mu_B$, extracted from neutron scattering data. In both $Sr_2YRu_{1-u}Cu_uO_6$ and $Ba_2GdRu_{1-u}Cu_uO_6$ the Ru orders ferromagnetically in the $a-b$ planes with the sheet magnetization alternating in direction as one moves along the c axis, forming a net antiferromagnetic structure. We find no evidence of a Ru signature in the magnetic resonance data anywhere in the range from 3 to 300 K, a result which is consistent with the electrons being itinerant. Attempts to detect Ru magnetic resonances in various other materials have also failed. Since in $Sr_2YRu_{1-u}Cu_uO_6$ the magnetic moments of the Ru and the Cu are ordered at low temperatures, its superconductivity is inconsistent with a spin-fluctuation pairing model.

DOI: 10.1103/PhysRevB.63.214412 PACS number(s): 74.72.−h, 74.25.Ha, 74.90.+n

I. INTRODUCTION

The rare-earth ruthenates $A_2R\text{RuO}_6$, with $A=$ Sr or Ba and R being a rare-earth ion (Fig. 1), can exhibit high-temperature superconductivity when doped with Cu on Ru sites, although they have no cuprate planes.[1–3] Our measurements indicate that $Sr_2YRu_{1-u}Cu_uO_6$ does superconduct at an onset temperature of $\approx$45 K,[4–6] although $Ba_2GdRu_{1-u}Cu_uO_6$ *does not superconduct*.[4] Furthermore, $Sr_2HoRu_{1-u}Cu_uO_6$ has been reported to superconduct as well,[7] suggesting that many elements of the class will superconduct, including perhaps even the $R=$ Cm and Am compounds.

In this paper, we report studies of nonsuperconducting Ba_2GdRuO_6 and superconducting Sr_2YRuO_6, both doped with Cu_{Ru} (Cu replacing Ru)[8] to identify which features of the dc susceptibility, the surface resistance, and the magnetic resonance data can be assigned to Cu, Gd, and Ru (as functions of temperature T and applied magnetic field **H**). We also report neutron diffraction spectra of Cu-doped Sr_2YRuO_6 which clarify the magnetic behaviors of the Ru and the Cu ions.

A. Cuprate-plane-based models

Cuprate-plane theories of high-temperature superconductivity, strictly speaking, have no application to this class of

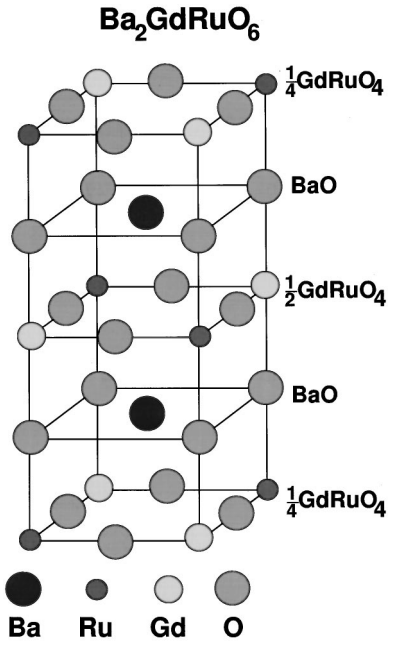

FIG. 1. Crystal structure of ideal $Ba_2GdRu_{1-u}Cu_uO_6$. This is only one fourth of a unit cell. In $Sr_2YRu_{1-u}Cu_uO_6$, the Ba has been replaced by Sr and the Gd by Y.

materials, since these materials have no cuprate planes. (The neutron diffraction studies of $Sr_2YRu_{1-u}Cu_uO_6$ reported here show $<1\%$ contaminant phases of any kind.[9,10]) Consequently it appears that cuprate planes may not be essential to the high-temperature mechanism of superconductivity.

Moreover, the *magnetic properties of the rare-earth elements, including* Gd, *are irrelevant* in most cuprate-plane models: both $Ba_2GdRu_{1-u}Cu_uO_6$ and $Sr_2YRu_{1-u}Cu_uO_6$ compounds should superconduct, if either does. However, $Sr_2YRu_{1-u}Cu_uO_6$ [with its two layers $(SrO)_2$ and $YRu_{1-u}Cu_uO_4$] does superconduct, but $Ba_2GdRu_{1-u}Cu_uO_6$ [with its two layers $(BaO)_2$ and $GdRu_{1-u}Cu_uO_4$] does not.[4] The fact that $Ba_2GdRu_{1-u}Cu_uO_6$, with $L=0$ magnetic Gd, does not superconduct, but $Sr_2YRu_{1-u}Cu_uO_6$, with nonmagnetic Y, does superconduct, suggests that $Sr_2YRu_{1-u}Cu_uO_6$ and $Ba_2GdRu_{1-u}Cu_uO_6$ may have physics in common with the homologues of two-layer $Nd_{2-z}Ce_zCuO_4$, where the $L=0$ (*s*-state) magnetic ions Gd (Refs. 11–14) and Cm (Ref. 15) form homologues that *do not superconduct*, while the other magnetic rare-earth ions (those with $L>0$ that do produce $Nd_{2-z}Ce_zCuO_4$ homologues) form materials that *do superconduct*. From the perspective of conventional cuprate-plane superconductivity, the $L=0$ ions Gd or Cm should not cause the destruction of superconductivity in either the $Nd_{2-z}Ce_zCuO_4$ homologues ($Gd_{2-z}Ce_zCuO_4$ or $Cm_{2-z}Th_zCuO_4$), or in the $Sr_2YRu_{1-u}Cu_uO_6$ homologue ($Ba_2GdRu_{1-u}Cu_uO_6$)—as they do. Note that the compounds with $L\neq 0$ trivalent magnetic ions, unlike those with $L=0$ Gd or Cm, do produce superconductivity in the same crystal structures: $Nd_{2-z}Ce_zCuO_4$ superconducts, and, although very few of the O_6 ruthenates (i.e., $Sr_2YRu_{1-u}Cu_uO_6$ homologues) have been fabricated yet, the one homologue with a magnetic rare-earth ion (Ho) that does not have $L=0$, $Sr_2HoRu_{1-u}Cu_uO_6$, has been reported to superconduct.[16,17]

Of course, conventional (e.g., cuprate plane) theories offer no explanation of the failure of $Gd_{2-z}Ce_zCuO_4$, $Cm_{2-z}Th_zCuO_4$, or $Ba_2GdRu_{1-u}Cu_uO_6$ to superconduct, because an essential element of those theories is the assumption that no magnetic rare-earth ion breaks Cooper pairs—as the $L=0$ magnetic rare-earth ions Gd (or Cm) must (and do in our picture[18]), see below. Hence conventional cuprate-plane theory cannot explain why $Sr_2YRu_{1-u}Cu_uO_6$ superconducts while $Ba_2GdRu_{1-u}Cu_uO_6$ does not, and cannot account for the failure of $Gd_{2-z}Ce_zCuO_4$ (Refs. 11–14) or $Cm_{2-z}Th_zCuO_4$,[15] or of the ruthenate $Ba_2GdRu_{1-u}Cu_uO_6$ to superconduct.

B. Oxygen model

The oxygen model predicts that magnetic rare-earth ions break Cooper pairs,[19] whenever the pairs are within range, i.e., within a nearest-neighbor distance of the magnetic ion—unless the rare-earth ion is crystal-field split. (Such splitting of the rare-earth's energy levels renders the ion impotent as a pair-breaker due to its inability to recoil.) Thus, the oxygen picture places the superconducting condensate of $Sr_2YRu_{1-u}Cu_uO_6$ in the SrO layers, and predicts that the Gd homologues (and Cm homologues, if they can be formed) of the superconducting $Sr_2YRu_{1-u}Cu_uO_6$ materials will not superconduct, because $L=0$ and $J\neq 0$ Gd (and Cm) are not crystal-field split and hence are pair breakers in these (and other) two-layer compounds. The compounds with $L\neq 0$ rare-earth ions are expected to superconduct, since the ions' levels are split by the crystal-field, and crystal-field splitting inhibits the pair breaking.

Another material which definitely follows the oxygen model is $PrBa_2Cu_3O_7$: Pr on the Ba site kills the superconductivity, although perfect $PrBa_2Cu_3O_7$ superconducts.[20] This implies that the cuprate-plane in between the two layers of Pr and of BaO does not contain the primary hole-condensate, and hence that the *primary* superconductivity of $PrBa_2Cu_3O_7$ must be in its charge-reservoir (CuO or BaO) layers, not in its cuprate planes.

In this paper we show that the data are consistent with our oxygen model of high-temperature superconductivity[21] in both superconducting $Sr_2YRu_{1-u}Cu_uO_6$ and nonsuperconducting $Ba_2GdRu_{1-u}Cu_uO_6$.

II. SAMPLE PREPARATION AND METHOD

The sample preparation techniques are discussed in detail in Refs. 1–3. In brief, polycrystalline $Sr_2YRu_{1-u}Cu_uO_6$ or $Ba_2GdRu_{1-u}Cu_uO_6$ samples were fabricated from stoichiometric compositions of $SrCO_3$ (or $BaCO_3$), Y_2O_3 (Gd_2O_3), RuO_2, and CuO using solid-state reaction techniques. The powders were mixed thoroughly, and then calcined in air at 1000 °C for several days. The reaction products were ground, pressed into pellets, and sintered in a mixture of 70% O_2 and 30% Ar at 1380 °C for 12 h. The resulting samples were then characterized by scanning electron microscopy, energy dispersive x-ray analysis, and x-ray diffraction.

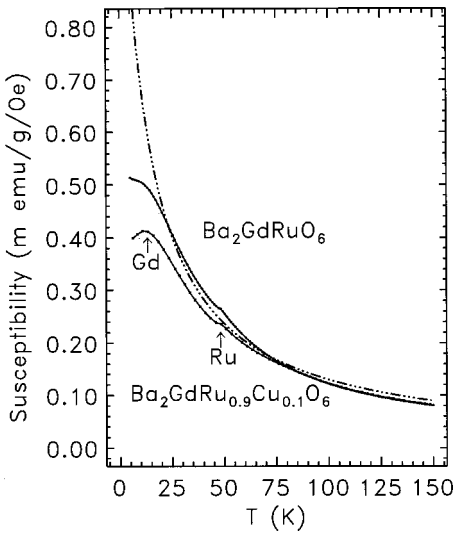

FIG. 2. Magnetic susceptibility (in m emu/g/Oe) of Ba_2GdRuO_6 and $Ba_2GdRu_{0.9}Cu_{0.1}O_6$ *versus* temperature in K. The Néel temperatures of Ru and Gd are indicated by arrows. These data were taken with small fixed fields in small temperature steps. The Ru ordering is indicated by a small peak in the susceptibility, and the Gd ordering produces a large peak at lower temperature. The Cu ordering at ~86 K is not obvious here. The chained line varies as $1/(T+10.86\,\mathrm{K})$.

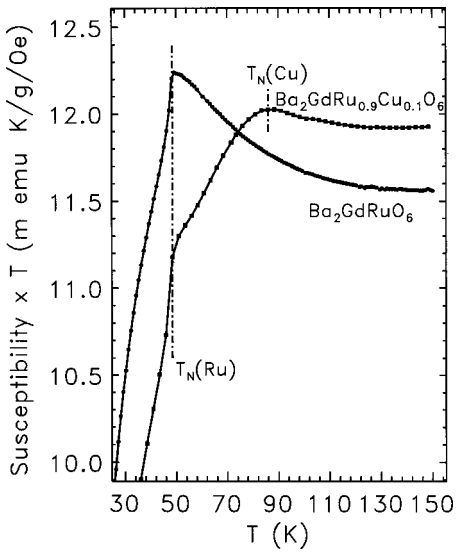

FIG. 3. Susceptibility times temperature of (a) Ba_2GdRuO_6 and (b) $Ba_2GdRu_{0.9}Cu_{0.1}O_6$ against temperature T in K. We noticed that the susceptibility of the sample with $u=0.1$ was field-dependent below ~86 K, and so multiplied the data of Fig. 2 by the temperature T. Note the transition temperatures (chained lines) at ~48 K associated with Ru (a change of slope), and at ~86 K (a peak) associated with Cu. The ~86 K peak is not present in the material with no Cu ($u=0$).

III. MAGNETIC SUSCEPTIBILITY

The magnetic susceptibility measurements were carried out on a Quantum Design MPMS-XL SQUID magnetometer. The samples were cooled in zero applied field; and the field due to trapped flux was offset to zero (± 0.5 G). The field necessary to offset the trapped flux was determined by performing a field scan at a high temperature, well above any magnetic transition, in the paramagnetic state.

A. $Ba_2GdRu_{1-u}Cu_uO_6$

Figure 2 shows the magnetic susceptibility as a function of temperature for (nonsuperconducting) $Ba_2GdRu_{1-u}Cu_uO_6$ (for $u=0$ and $u=0.1$). This susceptibility is well represented, except at temperatures below ~20 K, by a function which varies as $1/(T+\theta)$, with $\theta \approx 10.86$ K.

Since Gd has by far the largest moment of the constituents, $\sim 7.94\mu_B$, the susceptibility data (Fig. 2) show clearly that the Gd orders antiferromagnetically at ~12 K, because the susceptibility at all temperatures above, but not below, ~20 K, for $H<1.8$ T, is linear in $1/(T+\theta)$. The closeup of the susceptibility data multiplied by temperature (Fig. 3) shows the general trends for both Ba_2GdRuO_6 and $Ba_2GdRu_{0.9}Cu_{0.1}O_6$, together with the Néel temperatures of Cu and Ru.

Because the high-temperature susceptibility varies almost as $1/T$ in Fig. 2, we multiplied the data by the temperature, in order to emphasize the high-temperature behavior, for both Ba_2GdRuO_6 and $Ba_2GdRu_{0.9}Cu_{0.1}O_6$ (see Fig. 3.) Notice that the Néel temperatures at ~48 K (due to Ru) and at ~86 K (due to Cu) are now clearly evident in $Ba_2GdRu_{0.9}Cu_{0.1}O_6$. Note that there is no evidence of order at or near ~86 K for $u=0$ (because the sample contains no Cu).

The magnetization data for Ba_2GdRuO_6 (and also for $Ba_2GdRu_{0.9}Cu_{0.1}O_6$) as functions of applied field at fixed temperatures are *very nearly* linear through $H=0$ for $\mu_0 H < 2$ T (Fig. 4), with no indication of the spontaneous net magnetization or the hysteretic behavior characteristic of either ferromagnetism or weak ferromagnetism. (For example, the linearity is good to ~4 parts in 10^6 at 25 K) Since the linearity persists down to ~2 K (the lowest measurement temperature), the Cu (for $T<86$ K), Ru (for $T<48$ K in $Ba_2GdRu_{1-u}Cu_uO_6$), and Gd ions (for $T<12$ K) are all antiferromagnetically ordered at low temperatures, rather than being weakly ferromagnetic.

Above ~48 K in $Ba_2GdRu_{1-u}Cu_uO_6$, the Gd resonance is extremely narrow, a fact that we attribute to exchange narrowing[22] due to paramagnetic fluctuations of the Ru sublattice. At ~48 K the Ru spins in $Ba_2GdRu_{0.9}Cu_{0.1}O_6$ (Fig. 5) are most likely ordered ferromagnetically in each a-b plane, as is the case for Sr_2YRuO_6.[4] The magnetization data indicate unequivocally that the Ru spins in $Ba_2GdRu_{1-u}Cu_uO_6$ are ordered antiferromagnetically overall, which we take as evidence that the ordering is the same as in $Sr_2YRu_{1-u}Cu_uO_6$: ferromagnetic a-b planes adjacent along the c axis are stacked antiferromagnetically. This structure has been determined for Sr_2YRuO_6 by neutron diffraction data[23–26] and confirmed by the neutron studies on $Sr_2YRu_{0.85}Cu_{0.15}O_6$. In addition, in $Ba_2GdRu_{0.9}Cu_{0.1}O_6$, the large Gd moments evidently order antiparallel to the Ru moments, because at high fields ($\mu_0 H > 2$ T) and at temperatures as low as 2 K (and spanning the Gd ordering temperature of ~12 K) a metamagnetic or spin-flop transition (Fig. 4) is observed both in Ba_2GdRuO_6 and in $Ba_2GdRu_{0.9}Cu_{0.1}O_6$ [as observed earlier in Sr_2YRuO_6 (Ref.

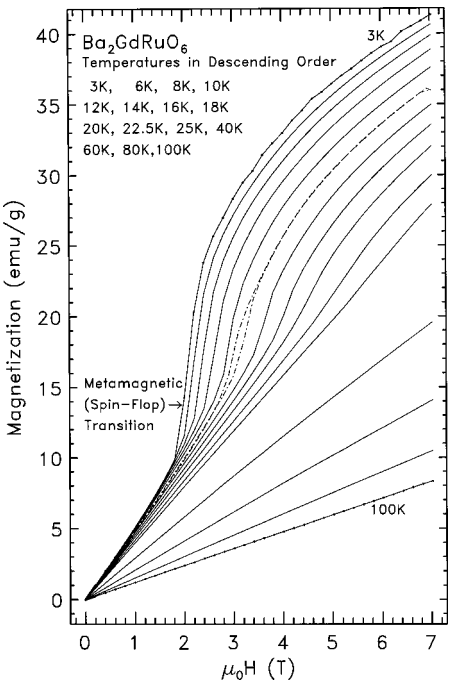

FIG. 4. Magnetization (in emu/g) of Ba_2GdRuO_6 vs applied magnetic field $\mu_0 H$ (in *T*), for various temperatures. The lines are for the different temperatures at which the data were taken, from 3 to 100 K (for 3 and 100 K, individual data points are given). The field steps were consistent for all scans. The dashed-dotted lines represent the hysteresis loop of the metamagnetic (spin-flop) transition for 14 K. These loops are not shown for other temperatures; only the $dH/dT>0$ curves are depicted. Metamagnetic transitions occur at low temperatures for $\mu_0 H > 1.8$ T, and are observable up to 25 K at higher fields. These data are very similar to those for $Ba_2GdRu_{0.9}Cu_{0.1}O_6$, which are not shown. The size of the increase in magnetization is consistent with this transition occurring in the Ru sublattice. The $T=0$ ferromagnetic saturation moment of the Ru sublattice is estimated to be ~17 emu/g (Ref. 27). The Gd sublattice orders antiferromagnetically with its Néel temperature $T_N \approx 12$ K, a result which eliminates the Gd sublattice as a potential source of the dramatic magnetization increase. For all temperatures and for all fields below the transition threshold, the magnetization is closely proportional to the applied field, as expected for an antiferromagnetic (or paramagnetic) system. For $T>20$ K, for both doped and undoped materials, the magnetization varies accurately as $H/(T+\theta)$, with $\theta = 10.86$ K. The proportionality constant estimated for $S=\frac{7}{2}$ Gd^{+3} is within 3% of the experimental value. This result also indicates that the large Gd moment (with its $T=0$ saturation moment of ≈73.83 emu/g) does not order at 48 K.

23)]. In this metamagnetic transition, the magnetization direction of the antiferromagnetic sublattice changes and *M* becomes abruptly nonlinear in *H*. The metamagnetic spin-flop transition is necessarily in the Ru sublattice, which is antiferromagnetically ordered overall, because it occurs in Cu-free Ba_2GdRuO_6 for temperatures greater than the Gd ordering temperature of ~12 K. [The size of the field-induced change of magnetization at 3 K, ~14 emu/g, is nearly equal to the assumed saturation moment of the Ru sublattice in $Ba_2GdRu_{0.9}Cu_{0.1}O_6$, ~17 emu/g (Ref. 27)]. As given by Battle and Macklin[23–26] and as confirmed by our own neutron diffraction results, the planes of the Ru sublattice are each ordered ferromagnetically in the *a*-*b* planes, but with adjacent layers in the *c* direction being antiferromagnetically aligned with respect to one another.

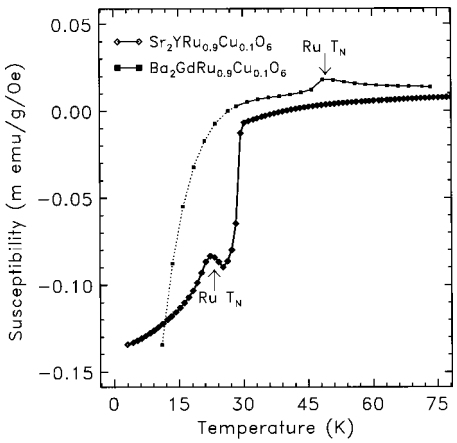

FIG. 5. Magnetic susceptibility (in m emu/g/Oe) vs temperature (in K) of $Ba_2GdRu_{0.9}Cu_{0.1}O_6$ (line with filled squares) and $Sr_2YRu_{0.9}Cu_{0.1}O_6$ (line with open diamonds). The line for $Ba_2GdRu_{0.9}Cu_{0.1}O_6$ has been displaced upwards by 0.01 m emu/g/Oe to facilitate presentation and has had the contribution of the $(T+\theta)^{-1}$ curve subtracted from the data of Fig. 4, leaving a dotted line at low temperatures. This negative-going line does not indicate superconductivity; it is a consequence of the magnetization's deviation from a $(T+\theta)^{-1}$ behavior at low temperatures. Note the similarity of the two Ru features, at ≈23 K for $Sr_2YRu_{0.9}Cu_{0.1}O_6$ and at ≈48 K for $Ba_2GdRu_{0.9}Cu_{0.1}O_6$. The difference at low temperatures of the data from the fit shows that the Gd sublattice orders at ~12 K. Had the Gd sublattice ordered at a higher temperature, for example, 48 K, the paramagnetic response would have deviated from this function for temperatures below 48 K. It did not. This means that the peaks seen at ~48 K are due to ordering of the Ru sublattice.

B. $Sr_2YRu_{1-u}Cu_uO_6$

The neutron data analyses of $Sr_2YRu_{1-u}Cu_uO_6$ (to be discussed in Sec. IV) assumed that the Ru moments are aligned antiparallel to the Cu moments,[28] namely, in a ferrimagnetic Ru-Cu structure for temperatures below the Ru ordering onset temperature of ~23 K (see Fig. 5). At this temperature, the Ru spins exhibit ferromagnetic order in each Ru plane.[4] Adjacent ferromagnetic planes along the *c* axis are antiferromagnetically ordered in $Sr_2YRu_{1-u}Cu_uO_6$.[4] Figure 6 shows magnetization data as a function of temperature for $Sr_2YRu_{0.85}Cu_{0.15}O_6$, and clearly shows (i) a Ru peak around 23 K, (ii) full superconductivity at ~30 K, and (iii) a peak attributable to the Cu Néel temperature near ~65 K.

IV. NEUTRON SPECTROSCOPY

A. Experimental method

Neutron diffraction data for $Sr_2YRu_{1-u}Cu_uO_6$ were collected using the high resolution powder diffractometer at the University of Missouri Research Reactor. (Measurements on the $Ba_2GdRu_{1-u}Cu_uO_6$ material were not possible because

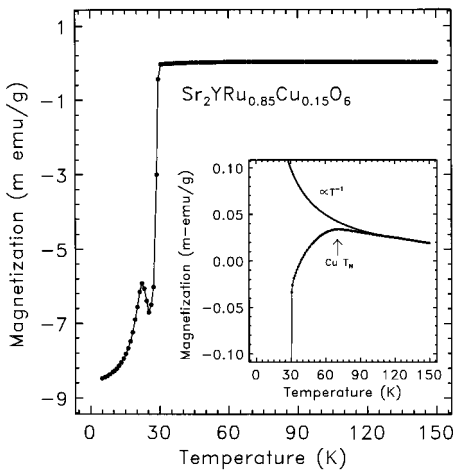

FIG. 6. Magnetization (in m emu/g) against temperature (in K) of $Sr_2YRu_{0.85}Cu_{0.15}O_6$, showing (i) a Ru peak near 23 K, (ii) full superconductivity at ~30 K, and (iii) a visible peak (see inset) associated with the Cu Néel temperature at ~65 K. Note the T^{-1} behavior above $T \approx 90$ K.

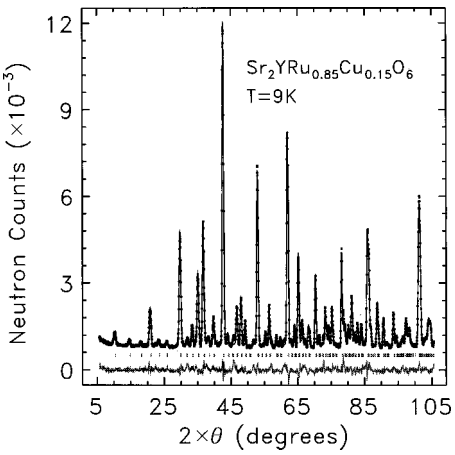

FIG. 7. Neutron diffraction spectrum of $Sr_2YRu_{0.85}Cu_{0.15}O_6$ vs 2θ for a temperature of 9 K. The bottom line is the residual. The tic marks indicate the composite nuclear and magnetic scattering angles. There are no unidentified peaks in the spectrum. The small residual counts indicate that the sample is phase pure.

of the large neutron absorption cross sections of the common Gd isotopes.) This instrument uses focusing neutron optics (from a bent Si crystal monochromator) and a position-sensitive detector. In order to not worsen the resolution, the sample diameter must be kept small. Approximately 1 g of material was mounted in a thin-walled vanadium sample holder. This was, in turn, mounted in a helium-filled aluminum can which attaches to the cold finger of a Leybold-Hereaus closed-cycle refrigerator capable of descending to roughly 9 K. The diameter of the aluminum can and surrounding heat shields is large enough that all of the Bragg scattered neutrons from these parts are rejected by the oscillating radial collimator. The position-sensitive detector spans 20° (2θ), and a full scan consists of measurements from 5° to 105° in five steps. This full scan was used only at two low temperatures, 9 and 40 K. The data from these measurements were used to fix the lattice parameters at intermediate temperatures, assuming a linear interpolation. The remaining data were collected for only the first 20° segment, 5°–25°, since the magnetic scattering is only observable in the low angle region.

Using the high-resolution powder diffractometer, neutron diffraction measurements were carried out on $Sr_2YRu_{0.85}Cu_{0.15}O_6$, which we expected to be more likely to exhibit phase inhomogeneity than samples having smaller Cu contents. The neutron data indicated no detectable impurity phase at the 1% level.[2]

Figure 7 shows neutron scattering data for $Sr_2YRu_{1-u}Cu_uO_6$ with $u=0.15$, taken at the temperature 9 K. Scattering data taken at various temperatures *versus* the scattering angle 2θ are presented in Fig. 8, showing magnetic peaks at $2\theta=10.5°$ and 14.8° that disappear at temperatures above 80 K. (A model based on a purely *c*-axis moment produces a completely unsatisfactory result for fitting the neutron data: no calculated intensity is found for the strongest observed magnetic reflection. In addition, if the Ru moments were ordered antiferromagnetically along the *c* axis, then both muon sites would see zero magnetic field, contrary to the observations of ~3 kG for the one site, in the Sr_2YRuO_4 layer, and zero field for the other muon site, in the SrO layer. Moreover, unconstrained refinements, allowing a *c* component, yield moment values that are zero within experimental error.) The magnetic scattering peaks disappear as temperature increases.

The neutron data were refined using the Fullprof code, in the monoclinic $p21/n$ space group previously reported by Battle and Macklin.[23–26] The magnetic data were treated as a separate phase in the space group $p-1$, but with the cell

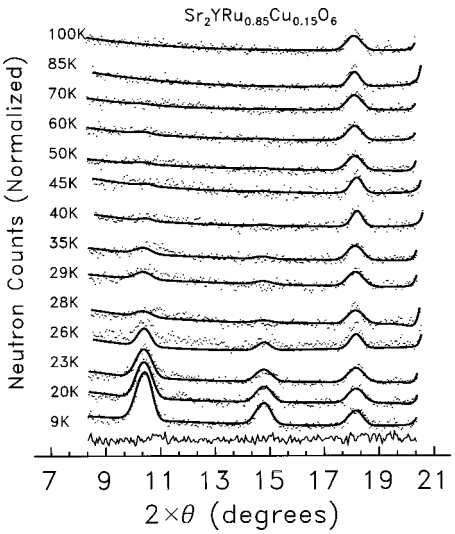

FIG. 8. Neutron scattering data, namely counts vs scattering angle 2θ. Note that the magnetic scattering peaks near $2\theta=10.5°$ and 14.8° are due to Ru and Cu magnetic scattering. The peak near 18° is nearly temperature-independent, and its intensity variation is due to different counting times. The bottom trace is the residual from the 9 K fit, which is typical of all these fits.

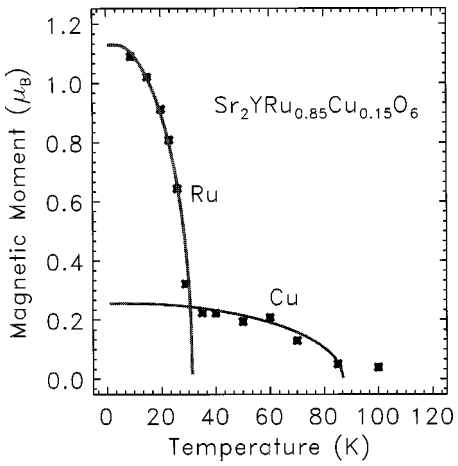

FIG. 9. Magnetic moment (in units of the Bohr magneton μ_B) of $Sr_2YRu_{0.85}Cu_{0.15}O_6$ against temperature. The neutron data were fitted with the two Brillouin functions shown, one that vanished around ~30 K, and another at around ~86 K. The zero-temperature magnetic moments were $\sim 1.7\mu_B$ for Cu and $\sim 1.6\mu_B$ for Ru. The curves intercept the magnetic moment axis at $0.255\mu_B$ and $1.13\mu_B$, respectively. (We have assumed that the ratio of the Cu intercept to the Cu content is the zero-temperature antiferromagnetic Cu moment; and that the difference of the Ru intercept and the Cu intercept give the Ru moment.)

parameters constrained to be the same as for the nuclear structure. The plotted neutron data therefore show a row of ''tic'' marks, corresponding to nuclear and magnetic scattering (Fig. 7). Below the inflection observed in the refined magnetic moment at ~30 K, the form factor for neutral Ru was employed because we know that the Ru is ordered (antiferromagnetically) at temperatures less than ~23 K. (Between ~23 and ~30 K the Ru exhibits short-ranged order.) Above ~30 K, the Cu^{+2} form factor was used because only the Cu is ordered (antiferromagnetically). Use of the neutral Ru form factor throughout resulted in only a very small change to the refined moment at the higher temperatures. As the temperature increased, the magnetic scattering decreased. Consequently the counting time was adjusted to improve the statistical accuracy at the higher temperatures. Although a nonzero moment was refined at 85 K and even at 100 K, the uncertainty at those points is too large to rule out a zero moment.

B. Magnetic moments of Ru and Cu in $Sr_2YRu_{1-u}Cu_uO_6$

Figure 9 shows the magnetic moments of Ru and Cu as functions of temperature for $Sr_2YRu_{0.85}Cu_{0.15}O_6$, as obtained from neutron data. Below ~30 K [the short-ranged ordering temperature of the Ru deduced from Ru Mössbauer measurements for $u=0.05$ (Refs. 4 and 5)], the magnetic moment increases in good agreement with a $J=\frac{3}{2}$ Brillouin function as the temperature decreases, reflecting the onset of Ru ordering.[29] Above ~30 K but below a critical temperature of ~86 K, we employ another $J=\frac{3}{2}$ Brillouin function due to the other magnetic species Cu.[30] Note that the magnetic moment of the Cu is $\sim 1.7\mu_B$, the intercept of the Cu curve at zero temperature divided by the Cu content of 0.15; and the zero-temperature magnetic moment of Ru (assumed to be antiparallel to a Cu moment on the same type of site) is $\sim 1.6\mu_B$, where μ_B is the Bohr magneton.[30] (If the Ru and Cu moments are ordered parallel to each other, the only other option, the Ru moment would be about $1\mu_B$, too small for the metamagnetic measurements above.) Clearly the Cu in Fig. 9, having a magnetization that is linear in H, is antiferromagnetically ordered for temperatures below ~86 K and the Ru is ordered (also antiferromagnetically) below ~23 K.

V. MICROWAVE SURFACE RESISTANCE AND RESONANCE

A. Experimental arrangement

Surface resistance and magnetic resonance measurements as a function of applied field and temperature were carried out in a microwave spectrometer of slightly unconventional design. This system did not employ magnetic field modulation. The microwave source (e.g., klystron or Gunn diode) was frequency locked to the resonant cavity containing the sample, by frequency modulating the source with a small-amplitude audio frequency signal. This yielded a modulated cavity response which was minimized with vanishing phase shift at the cavity resonance frequency. Using a phase-sensitive lock-in technique to monitor the detected rf signal reflected from the cavity, a filtered (approximately dc) correction signal was developed, and added to the audio frequency modulation. With proper adjustment of the lock-in phase, this feedback loop was stable, and the signal source precisely tracked any changes of the cavity frequency. The detected dc signal accurately included changes in the quality factor (Q) of the cavity due to field- or temperature-induced changes in the sample power dissipation. As a result, the spectrometer was sensitive only to changes in the dissipation (surface resistance or resonant absorption) of the sample, and was not sensitive to changes of the sample reactance. Changes in the reactance of superconducting samples as the temperature was varied through the transition temperature were indicated by changes in the cavity resonant frequency, which were observed, but were not recorded.

The sample was always small in size relative to the surface area of the cavity, and was mounted in either of two positions in the rectangular (TE_{101}) cavity. The resulting small sample filling-factor assured that the rf magnetic field intensity remained nearly constant, if the sample was brought into resonance, or if the surface resistance varied rapidly with field or temperature. When the sample was mounted on the bottom center of the cavity, the applied dc magnetic field could be rotated in the plane of the sample; and the dc magnetic field could be applied at any angle in the plane relative to the nearly uniform rf magnetic field of the cavity. Mounting a sample on the side wall of the cavity was useful when the sample was highly textured or crystalline. In this case, the applied magnetic field was normally applied at any angle relative to the sample plane, and anisotropy in the sample's response was easily obtained.

As the temperature was changed, the properties of the cavity varied slowly; these changes led to changes in the cavity coupling coefficient which were compensated for by a

cavity impedance-matching device. The nominal 100 mW power output level of the signal source was maintained, and was typically attenuated by 25–40 db before it was coupled into the cavity. The resulting rf current densities were varied from roughly 10^3 to $10^5\,A/\mathrm{cm}^2$. A broad-band solid-state microwave amplifier was used to amplify the low-level signal reflected from the cavity, prior to detection with a point-contact diode. In this way, the sample response could be reliably measured over wide ranges of applied field and temperature.

B. Magnetic excitations and selection rules

In the case of antiferromagnetism, two nondegenerate (for $q \neq 0$) magnon modes are generally expected, which are degenerate at $q=0$; the selection rules are such that the two modes can be independently excited, namely, with $\mathbf{H} \| \mathbf{J}$ (or $\mathbf{H} \perp \mathbf{H}_{\mathrm{rf}}$) and with $\mathbf{H} \perp \mathbf{J}$ (namely, $\mathbf{H} \| \mathbf{H}_{\mathrm{rf}}$). The derivations of these results are discussed in detail by Turov,[31] and with less detail by Morrish.[32] Note that the selection rule for paramagnetic resonance is that electron spin resonance is excited only with $\mathbf{H} \| \mathbf{J}$. It is also the case that weak ferromagnets have similar magnon modes and selection rules to those of the antiferromagnetic case.[33]

Although it is typically the case for antiferromagnets that the antiferromagnetic magnon modes fall in the infrared, for high symmetry materials (e.g., cubic lattices) the effective anisotropy fields are comparatively reduced, and so the magnon energies are lower—and may fall in the range of microwave frequencies. Since the Ba_2GdRuO_6 structure is nearly cubic,[34] both magnon modes could be probed with conventional microwave techniques.

C. Gd resonance of $Ba_2GdRu_{1-u}Cu_uO_6$

In Fig. 10 we present the results of our microwave surface resistance (magnetic resonance) measurements on Cu-free Ba_2GdRuO_6, as functions of temperature T and applied magnetic field $\mathbf{H}$, for a microwave frequency of 13 GHz. The resonance spectra are described as $\Delta R_s = R_s(\mathbf{H},T) - R_s(H=0,T)$, appropriate to a conducting material. In the event, as for $u=0$, the material is an insulator, the microwave magnetic field penetrates the material without significant attenuation.

The data in Fig. 10(a) are for the resonance configuration, namely $\mathbf{H} \| \mathbf{J}$, where $\mathbf{J}$ is the rf current density, and for an input power of 100 mW, attenuated by 40 db before being input to the cavity. Corresponding data for $\mathbf{H} \perp \mathbf{J}$ are in Fig. 10(b), which shows no evidence of the peak that dominates Fig. 10(a). Similar results for $Ba_2GdRu_{0.9}Cu_{0.1}O_6$ (for 30 db) and $Sr_2YRu_{0.85}Cu_{0.15}O_6$ (for 30 db) are presented in Figs. 11 and 12, respectively. Figures 11(a) and 11(b) for Cu-doped material are similar to Figs. 10(a) and 10(b) for Cu-free material, except that (i) Figs. 11(a) and 11(b) have low-H features associated with Cu, and (ii) Fig. 11(b) exhibits a very weak $g=2$ resonance feature below ~86 K (so weak that it is not visible in this figure, but is visible when the microwave frequency is increased to 32 GHz) that is similar to the Gd signal of Fig. 11(a), but is much weaker, and occurs

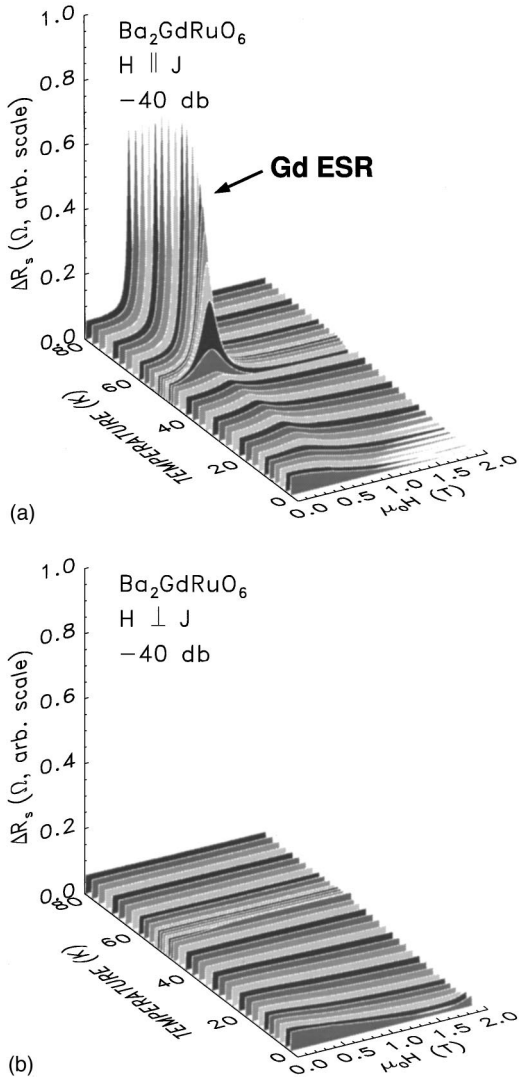

FIG. 10. Change in microwave surface resistance ΔR_s of Ba_2GdRuO_6 (a) for $\mathbf{H} \| \mathbf{J}$ and (b) for $\mathbf{H} \perp \mathbf{J}$, against temperature T (in K) and $\mu_0 H$ (in T), where $\mathbf{J}$ is the rf current density and $\mathbf{H}$ is the applied field. The microwave frequency is 13 GHz. The data were observed with 40 db attenuation of the rf power level. The four notable features of these spectra are (i) the Gd electron spin resonance (ESR) peak in (a) which broadens dramatically below about ~48 K, (ii) no Gd peak present in (b) here, but one is visible at 32 GHz (not shown), (iii) no Cu peak visible in (a) or (b), and (iv) no feature attributable to Ru in either (a) or (b). The data were taken at the temperatures indicated.

because the Gd is in an effective field whose direction differs from the applied field. $Sr_2YRu_{1-u}Cu_uO_6$ [Figs. 12(a) and 12(b)], having no Gd, does not exhibit a $g=2$ electron spin resonance.

Figures 10(a) and 11(a) feature prominent $g=2$ Gd resonance peaks in Ba_2GdRuO_6 and in $Ba_2GdRu_{6.9}Cu_{0.1}O_6$ which can be confirmed as Gd-related by their absence in the homologous Gd-free material $Sr_2YRu_{1-u}Cu_uO_6$ [Fig. 12(a)]. This Gd peak broadens dramatically at temperatures below ≈48 K and becomes nearly undetectable at this frequency, within a very small temperature range of about 0.5 K. The unusually narrow Gd resonance observed above ≈48 K is

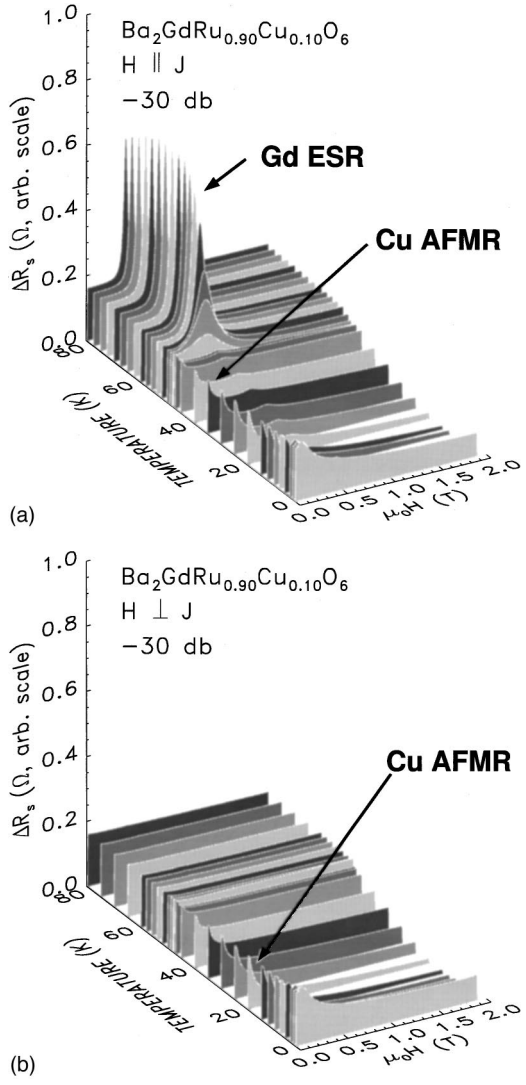

FIG. 11. Change in microwave surface resistance ΔR_s of $Ba_2GdRu_{0.9}Cu_{0.1}O_6$ against temperature T (in K) and $\mu_0 H$ (in T) for (a) $\mathbf{H} \| \mathbf{J}$ and (b) $\mathbf{H} \perp \mathbf{J}$, where $\mathbf{J}$ is the rf current density and $\mathbf{H}$ is the applied field. The microwave frequency is 13 GHz. The data were observed with 30 db attenuation of the rf power level. Note that in (a) the Gd ESR feature is present as in Fig. 10(a) and a Cu antiferromagnetic resonance (AFMR) peak (at low H) is also present, and in (b) there is a Cu resonance at low fields, proving that the Cu is antiferromagnetic, and contributes to the local field seen by the Gd, so that the Gd resonates in an otherwise forbidden configuration at 32 GHz (not visible here). There is no evidence of Ru in these data. The integrated intensities of the Gd peak and the Cu peak cannot be easily compared, but it is the case that the integrated intensity of the Cu peak at low temperatures is smaller than that of the Gd peak above 48 K. This means that the Cu peak is consistent with originating from the small content of Cu.

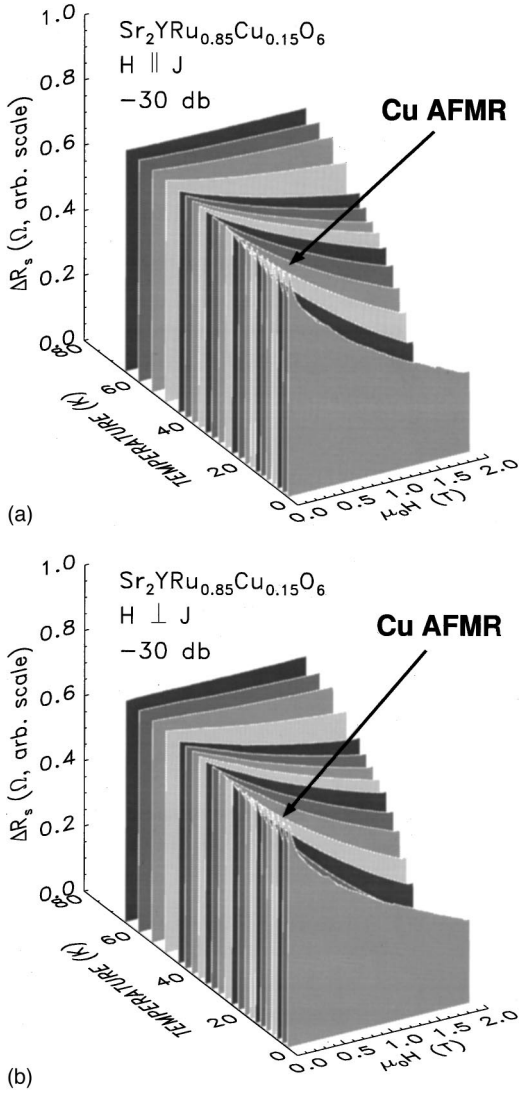

FIG. 12. Change in microwave surface resistance ΔR_s of $Sr_2YRu_{0.85}Cu_{0.15}O_6$ against temperature T (in K) and $\mu_0 H$ (in T) for (a) $\mathbf{H} \| \mathbf{J}$ and (b) $\mathbf{H} \perp \mathbf{J}$, where $\mathbf{J}$ is the rf current density and $\mathbf{H}$ is the applied field. The microwave frequency is 13 GHz. The notable features of these spectra, which were observed with 30 db attenuation of the rf power level, are the low-H Cu peaks present both in (a) and in (b), which indicate the antiferromagnetism of the Cu.

exchange narrowed by interaction with the paramagnetic Ru moments. Following the ordering at ~48 K, the Gd resonance is no longer exchange narrowed and becomes extremely broad and difficult to detect at low temperatures.

Figures 10(b) and 11(b) show that the Gd resonance peaks of Figs. 10(a) and 11(a) are absent for $\mathbf{H} \perp \mathbf{J}$ in Ba_2GdRuO_6, and are so weakly present in Fig. 11(b) for $Ba_2GdRu_{0.9}Cu_{0.1}O_6$ as to be visible only when the microwave frequency is increased to 32 GHz—for temperatures at which the Cu is ordered ($T < 86$ K).

D. Cu resonance of $Ba_2GdRu_{1-u}Cu_uO_6$

The spectra for Cu-doped $Ba_2GdRu_{0.90}Cu_{0.10}O_6$ are given in Fig. 11, and contain, in addition to the peak which corresponds to the $g=2$ Gd resonance of Fig. 10, a low-field feature indicative of a resonance for which the magnon energy gap $\hbar\omega(q=0)$ exceeds the microwave energy—a behavior that we have thought of as a resonance centered at a negative field. This feature is associated with Cu, and is certainly not present at the 1% level in undoped Ba_2GdRuO_6, a limit we

can set on the Cu impurity content of our undoped samples. As expected, it is also present in the Cu-doped material $Sr_2YRu_{0.85}Cu_{0.15}O_6$ (Fig. 12).

Since this Cu feature is present for $\mathbf{H}\perp\mathbf{J}$, as well as for $\mathbf{H}\|\mathbf{J}$[35] (Figs. 11 and 12), the Cu must be either weakly ferromagnetic or antiferromagnetic (magnetization linear in H), rather than either paramagnetic (magnetization linear in H), or ferromagnetic. (In Sec. III A, we showed that the Cu is antiferromagnetic.)

The Cu features of the resonance data were detected and persisted up to ~60 K, but proved undetectable at higher temperatures, although the ordered Cu magnetic moments are detected by neutrons up to ~86 K. (See Figs. 7, 8, and 9.)

E. Absence of a Ru resonance in either ruthenate

There are no identifiable Ru resonances, either paramagnetic or ordered, in our surface resistance spectra of either Ba_2GdRuO_6 (Fig. 10), $Ba_2GdRu_{1-u}Cu_uO_6$ (Fig. 11), or $Sr_2YRu_{1-u}Cu_uO_6$ (Fig. 12). Ru has been identified in magnetization, specific heat,[16] muon spin rotation, neutron diffraction, and Mössbauer data, however.[4,5,16] Indeed, since the closely related compounds RuO_2, $SrRuO_3$, and $Ba_3Ru_2NiO_9$ all fail to exhibit a Ru magnetic resonance signal in either the ordered (e.g., antiferromagnetic) or the disordered (e.g., paramagnetic) states, we do not expect one for the materials $Ba_2GdRu_{1-u}Cu_uO_6$ or $Sr_2YRu_{1-u}Cu_uO_6$ either.

F. Superconductivity of $Sr_2YRu_{1-u}Cu_uO_6$

The muon spin rotation measurements on the $Sr_2YRu_{1-u}Cu_uO_6$ compounds clearly exhibit bulk superconductivity which appears to become fully developed as the Ru moments order below ~30 K.[4,5] This ordering temperature is significantly below the onset temperature of ~45 K measured with microwaves. Moreover, the muon experiment showed that the flux in these sintered samples is very weakly pinned, suggesting extreme anisotropy.[4] Consequently, it is our view that the superconductivity can be described by isolated sheets of ''pancake'' vortices, as would be the case if the superconducting hole-condensate resides in the SrO layers, since the magnetism in the $YRu_{1-u}Cu_uO_4$ layers does not support superconductivity.

$Sr_2YRu_{1-u}Cu_uO_6$ is superconducting,[16] but the antiferromagnetic Cu resonance signal completely overwhelms the vortex dissipation for $u=0.15$ (see Figs. 9 and 12). Vortex dissipation is evident in this class of materials if the Cu-dopant concentration u is smaller, however.[4,5]

Unlike in $Sr_2YRu_{1-u}Cu_uO_6$ which superconducts, we have detected no superconductivity in $Ba_2GdRu_{1-u}Cu_uO_6$, which we attribute to Gd being an $L=0$ magnetic ion. $L=0$, $J\neq 0$ Gd, unlike $L\neq 0$ magnetic trivalent rare-earth ions, is not crystal-field split, and hence breaks Cooper pairs–thereby suppressing both pair formation and superconductivity.[36,37]

VI. ASSIGNMENTS OF THE EXPERIMENTAL FEATURES TO IONS

A. The Cu feature at ≈86 K

Figure 3 shows the magnetic susceptibilities (times temperature) of Ba_2GdRuO_6 and $Ba_2GdRu_{1-u}Cu_uO_6$. The Cu feature is clearly at ≈86 K for $Ba_2GdRu_{0.9}Cu_{0.1}O_6$ (and absent for Cu-less Ba_2GdRuO_6). Comparable data are found for $Sr_2YRu_{1-u}Cu_uO_6$ (Fig. 6). The Cu in $Ba_2GdRu_{1-u}Cu_uO_6$ is also detected in the surface resistance (magnetic resonance) near zero applied field (for $\mathbf{H}\|\mathbf{J}$ and $\mathbf{H}\perp\mathbf{J}$) in both Figs. 11(a) and 11(b) and in $Sr_2YRu_{1-u}Cu_uO_6$ (for $\mathbf{H}\|\mathbf{J}$ and $\mathbf{H}\perp\mathbf{J}$) in Figs. 12(a) and 12(b). Finally the neutron data for $Sr_2YRu_{0.85}Cu_{0.15}O_6$ reveal the Cu ordering from ≈86 K down to lower temperatures (Fig. 9). Independently, the magnetic resonance (surface resistance), susceptibility, and neutron diffraction all show that the ≈86 K feature is Cu.

While, at first glance, it may seem unusual that a few percent Cu orders, there is ample precedent for even orders-of-magnitude lower concentrations of magnetic ions to become ordered by the Ruderman-Kittel-Kasuya-Yosida interaction.[38,39]

Gd in $Ba_2GdRu_{1-u}Cu_uO_6$ is paramagnetic (and continuously so) down through ≈86 K and ≈48 K, and down to temperatures <20 K. Gd detects something, namely, Ru, that orders—and changes Gd's magnetic resonance relaxation (surface resistance) at ≈48 K. The magnetization data also indicate that the ≈48 K transition is not due to Gd. Gd has a $7.94\,\mu_B$ magnetic moment which would be too large to explain the magnetic data if it were ordered much above ~12 K. Hence, our experiments require us to assign the antiferromagnetic ordering of Cu to ≈86 K, of Ru to ≈48 K, and of Gd to ≈12 K in $Ba_2GdRu_{1-u}Cu_uO_6$.

B. The Ru feature in $Sr_2YRu_{1-u}Cu_uO_6$ at 23 to 30 K

In Fig. 5, the Ru shows up in the temperature-dependent magnetization data of $Sr_2YRu_{1-u}Cu_uO_6$ as a peak at ≈23 K. It also manifests itself in muon spin rotation, where the most intense muon relaxation rate drops rapidly with increasing temperature around ≈30 K while the muon precession frequency increases abruptly with increasing temperature in the SrO layer.[4] (The drop in the muon precession frequency below the superconducting onset temperature indicates flux expulsion.)

The ^{99}Ru Mössbauer absorption of $Sr_2YRu_{1-u}Cu_uO_6$ is an 18-line spectrum for low temperatures (see Fig. 12 of Ref. 4), and the 18-fold splitting reduces to a single line above ≈30 K, indicating that the 23 to 30 K feature is definitely Ru.

C. The remaining features in $Ba_2GdRu_{1-u}Cu_uO_6$

The last two features of $Ba_2GdRu_{1-u}Cu_uO_6$ are (i) the susceptibility measurements which indicate a transition at ≈48 K and (ii) the microwave magnetic resonance (surface resistance) which features a narrow strong peak (for $T>48$ K) that weakens and is dramatically broadened below 48 K, but persists to lower temperatures. We assign the ≈48 K feature of the magnetic resonance and of the magnetization data to Ru, and the ≈12 K feature of the magnetization data to Gd.

VII. CONCLUSIONS

A. $Sr_2YRu_{1-u}Cu_uO_6$

Perhaps the most interesting conclusion to be drawn from these data is that Cu ions in the $Sr_2YRu_{1-u}Cu_uO_6$ supercon-

ducting compound are ordered antiferromagnetically for temperatures below ~86 K, although the material has a superconducting onset temperature of ~45 K. The sample is very pure and single-phased, ruling out the possibility that the broadened superconducting transition at ~25 to ~45 K (see Fig. 2 of Ref. 4.) is related to phase inhomogeneity. Instead we suggest that the broadening may be attributable to fluctuating Ru moments that break pairs. Below about ~30 K, these fluctuations diminish rapidly, and finally, at ~23 K, the Ru spins order (ferromagnetically in the *a*-*b* plane, but antiferromagnetically along the *c* axis), allowing the formation of a fully developed superconducting state (in the SrO layers).

Since this material (in the superconducting state) is also antiferromagnetically ordered, one might assume that the Ginzburg conditions for magnetic superconductors[40,41] would apply. In the present case, however, the Ginzburg conditions are actually irrelevant, since muon spin rotation measurements indicate that the superconducting hole-condensate resides in the nonmagnetic SrO layers. Specifically, muon spin rotation data[4] exhibit (i) clear evidence of flux expulsion (typical of type-II superconductivity), for muons stopped in the SrO layers, which is not observed for muons in the magnetically ordered $YRu_{1-u}Cu_uO_4$ layers and (ii) extremely weak pinning of the vortices (see Fig. 11 of Ref. 4). Both of these results are consistent with a system of isolated sheets of pancake vortices—precisely what is expected if the superconducting hole-condensate resides in the nonmagnetic SrO layers, while the $YRu_{1-u}Cu_uO_4$ layers are ferromagnetically ordered in the *a*-*b* planes and antiferromagnetically ordered in adjacent $YRu_{1-u}Cu_uO_4$ layers along the *c* axis. (If the $YRu_{1-u}Cu_uO_4$ layers were superconducting, then they would expel flux and the field in the SrO layers would increase below the transition temperature.) Hence adjacent $YRu_{1-u}Cu_uO_4$ layers contain opposing ~3 kG magnetic fields at the muon sites. The net dipole field cancels in the SrO layer, since the magnetic polarization direction reverses between adjacent $YRu_{1-u}Cu_uO_4$ layers.[4,5]

A further conclusion is that neither Cu nor Ru in the $YRu_{1-u}Cu_uO_4$ layer provides a spin-fluctuation pairing center which produces superconductivity in that layer, because, as the temperature approaches zero, the superconductivity does not vanish, but the small fluctuations associated with the ordered moments do: The Cu spins are ordered at temperatures both above and below the bulk superconducting transition temperature of ~45 K, and the Ru spins are ordered at ~23 K.

B. $Ba_2GdRu_{1-u}Cu_uO_6$

Gd electron spin resonance has been used as a local probe of the magnetic environment of $Ba_2GdRu_{1-u}Cu_uO_6$: (i) the Gd electron spin resonance was exchange narrowed by paramagnetic Ru, (ii) the resonance was broadened by the ordering of Ru, and (iii) the Gd electron spin resonance was modified also by ordered (antiferromagnetic) Cu which produced a small Gd signal for $\mathbf{H}\|\mathbf{J}$ at temperatures below the Cu ordering temperature of ~86 K. In this configuration, electron spin resonance is normally forbidden [see Fig. 11(b)].

Gd orders antiferromagnetically at 12 K, and Ru is also antiferromagnetic at ~48 K in this material.

C. Implications

A significant implication of our results occurs because the magnetic resonance feature we have identified as due to Cu in both $Ba_2GdRu_{1-u}Cu_uO_6$ and $Sr_2YRu_{1-u}Cu_uO_6$ has also been identified in $GdSr_2Cu_2RuO_8$—where it has been assigned by Fainstein *et al.* to Ru.[3] Our evidence suggests that this feature is actually due to Cu, which implies that their interpretations of the ≈45 K $GdSr_2Cu_2RuO_8$ superconductivity and also the $\approx 45\,\mathrm{K}\ Gd_{2-z}Ce_zSr_2Cu_2RuO_{10}$ superconductivity as due to CuO_2 planes may have to be revised—which could pose a broader problem for cuprate-plane interpretations. Such a reinterpretation is expected to be compatible with the viewpoint expressed in Ref. 42: that the SrO layers superconduct in all of these compounds, except when the $L=0$ Gd is a pair-breaker adjacent to the superconducting (SrO or BaO) layer, as is the case in $Ba_2GdRu_{1-u}Cu_uO_6$. (Recall that $Sr_2YRu_{1-u}Cu_uO_6$, which is a homologue of $Ba_2GdRu_{1-u}Cu_uO_6$ but without pair-breaking $L=0$, $J\neq 0$ Gd, also superconducts at an onset of ~45 K.)

Finally, the Cu ions in $Ba_2GdRu_{1-u}Cu_uO_6$ behave similarly to those in $Sr_2YRu_{1-u}Cu_uO_6$, although $Ba_2GdRu_{1-u}Cu_uO_6$ does not superconduct—which we attribute to the fact that Gd has $L=0$ and is a magnetic pair breaker which is not crystal-field split. Our picture implies that the superconductivity in $Sr_2Gd_vY_{1-v}Ru_{1-u}Cu_uO_6$ will be depressed as v increases, and the depression of T_c should approximately follow Abrikosov-Gor'kov theory.[43]

ACKNOWLEDGMENTS

We are grateful to the U.S. Department of Energy (MISCON Grant No. De-FG0290ER45427), U.S. Army Research Office (Grant No. DAAG55-97-1-0387), the U.S. Office of Naval Research (Contract No. N00014-98-10137), and the ROC National Science Grant No. NSC87-2212-M-110-006 for their support. We are thankful to Q. Cai for his role in the neutron data analyses.

*Permanent address.

†Deceased.

[1] M. K. Wu, D. Y. Chen, F. Z. Chien, S. R. Sheen, D. C. Ling, C. Y. Tai, G. Y. Tseng, D. H. Chen, and F. C. Zhang, Z. Phys. B: Condens. Matter **102**, 37 (1996).

[2] D. Y. Chen, F. Z. Chien, D. C. Ling, J. L. Tseng, S. R. Sheen, M. J. Wang, and M. K. Wu, Physica C **282–287**, 73 (1997).

[3] A. Fainstein, E. Winkler, A. Butera, and J. Tallon, Phys. Rev. B **60**, 12 597 (1999).

[4] H. A. Blackstead, J. D. Dow, D. R. Harshman, M. J. DeMarco,

M. K. Wu, D. Y. Chen, F. Z. Chien, D. B. Pulling, W. J. Kossler, A. J. Greer, C. E. Stronach, E. Koster, B. Hitti, M. Haka, and S. Toorongian, Eur. Phys. J. B **15**, 649 (2000).

[5] D. R. Harshman, W. J. Kossler, A. J. Greer, C. E. Stronach, E. Koster, B. Hitti, M. K. Wu, D. Y. Chen, F. Z. Chien, H. A. Blackstead, and J. D. Dow, Int. J. Mod. Phys. B **13**, 3620 (1999).

[6] D. R. Harshman, W. J. Kossler, A. J. Greer, C. E. Stronach, E. Koster, B. Hitti, M. K. Wu, D. Y. Chen, F. Z. Chien, H. A. Blackstead, and J. D. Dow, Physica B **289–290**, 360 (2000).

[7] M. K. Wu, D. Y. Chen, F. Z. Chien, D. C. Ling, Y. Y. Chen, and H. C. Ren, Int. J. Mod. Phys. B **13**, 3585 (1999).

[8] Gd^{+3} has orbital angular momentum quantum number $L=0$, and so does not experience crystal-field splitting.

[9] There is no possibility of successful invocation of a *filamentary model* exploiting $YSr_2Cu_3O_7$, even if it could be formed, for the following reasons. This is the one other material known to superconduct and to be made of the available ions, but (i) $YSr_2Cu_3O_7$ forms only under high pressure (Ref. 10), which is not part of the preparation process employed for these samples, (ii) $Sr_2YRu_{1-u}Cu_uO_6$ exhibits bulk superconductivity for concentrations $u=0.05$, 0.10, and 0.15 well below any possible percolation threshold for $YSr_2Cu_3O_7$, and (iii) the neutron data presented here show that $Sr_2YRu_{1-u}Cu_uO_6$ forms without appreciable (<1%) contaminant phase content, eliminating the $YSr_2Cu_3O_7$ impurity-phase model of the superconductivity.

[10] Y. Cao, T. L. Hudson, Y. S. Wang, S. H. Xu, Y. Y. Xue, and C. W. Chu, Phys. Rev. B **58**, 11 201 (1998).

[11] J. D. Thompson, S.-W. Cheong, S. E. Brown, Z. Fisk, S. B. Oseroff, M. Tovar, D. C. Vier, and S. Schultz, Phys. Rev. B **39**, 6660 (1989).

[12] H. Ishii, T. Koshizawa, T. Hanyu, and S. Yamaguchi, Jpn. J. Appl. Phys. **32**, 1070 (1993).

[13] M. Braden, W. Paulus, A. Cousson, P. Vigoreaux, G. Heger, A. Goukassov, P. Bourges, and D. Petitgrand, Europhys. Lett. **25**, 625 (1994).

[14] U. Asaf and I. Felner, Solid State Commun. **94**, 873 (1995).

[15] L. Soderholm, S. Skanthakumar, and C. W. Williams, Phys. Rev. B **60**, 4302 (1999).

[16] M. K. Wu, D. Y. Chen, F. Z. Chien, D. C. Ling, Y. Y. Chen, and H. C. Ren, Int. J. Mod. Phys. B **13**, 3585 (1999).

[17] $Sr_2HoRu_{1-u}Cu_uO_6$ should superconduct if the magnetic field in the SrO layer is sufficiently small.

[18] We shall refer to this model for inorganic compounds as the ''oxygen'' model, although sulfur can play the role of oxygen in some organic superconductors.

[19] H. A. Blackstead and J. D. Dow, Phys. Rev. B **51**, 11 830 (1995).

[20] H. A. Blackstead and J. D. Dow, Solid State Commun. **115**, 137 (2000).

[21] J. D. Dow, Proc. SPIE **2999**, 335 (1997).

[22] C. Kittel, *Introduction to Solid State Physics*, 7th ed. (Wiley, New York, 1996), p. 510.

[23] P. D. Battle and W. J. Macklin, J. Solid State Chem. **52**, 138 (1984).

[24] P. D. Battle and W. J. Macklin, J. Solid State Chem. **54**, 245 (1984).

[25] P. D. Battle, J. B. Goodenough, and R. Price, J. Solid State Chem. **46**, 234 (1983).

[26] References 23 and 24 find the Ru moments aligned in the $a-b$ planes of Sr_2YRuO_6 and Ca_2YRuO_6, while the Ru moments are along the c axes of Ca_2LaRuO_6 and Ba_2LaRuO_6 (Ref. 25). Our neutron measurements (by W. B. Yelon and M. X. Ching) indicate that the Ru moments are in the $a-b$ planes of $Sr_2YRu_{1-u}Cu_uO_6$ as well.

[27] The assumed saturation moment for the Ru sublattice of $Ba_2GdRu_{0.9}Cu_{0.1}O_6$, ~17 emu/g, is taken to be the number of spins per gram multiplied by $1.6\mu_B$. See Sec. IV B. The $1.6\mu_B$ is determined by neutron diffraction of $Sr_2YRu_{0.85}Cu_{0.15}O_6$, but this is justified by the near equality of the field-induced change of magnetization of $Ba_2GdRu_{0.9}Cu_{0.1}O_6$, ~15 emu/g, and the assumed saturation moment (~17 emu/g).

[28] Y. Doi and Y. Hinatsu, J. Phys.: Condens. Matter **11**, 4813 (1999).

[29] We interpret the low-temperature moments as due to the difference of 0.85 times the Ru moment and 0.15 times the Cu moment. The high-temperature moment is due to Cu.

[30] We think that the Cu is Cu^{+Z} where we have $Z>2$ because the ionization potential of Ru^{+5} is comparable with that of Cu^{+4}, indicating that the Cu on a Ru^{+5} site will most likely assume a charge state with $Z>2$.

[31] E. A. Turov, *Fizicheskiye Svoysiva Magnitouporyadochennykh Kristallov* (Physical Properties of Magnetically Ordered Crystals), translated by A. Tybulewicz and A. Schomet (Academic, New York, 1965), p. 64.

[32] A. H. Morrish, *The Physical Principles of Magnetism* (Wiley, New York, 1965), p. 620.

[33] E. A. Turov, *The Physical Principles of Magnetism* (Ref. 32), p. 157.

[34] S. H. Kim and P. D. Battle, J. Solid State Chem. **44**, 174 (1995).

[35] In principle, the $\mathbf{H}\perp\mathbf{J}$ feature is compatible with weak ferromagnetism as well as anti-ferromagnetism; we exclude weak ferromagnetism based on our magnetization data, which are linear in $\mathbf{H}$.

[36] H. A. Blackstead and J. D. Dow, Phys. Rev. B **55**, 6605 (1997).

[37] H. A. Blackstead and J. D. Dow, Physica C **282–287**, 1005 (1997).

[38] K. Yosida, Phys. Rev. **106**, 893 (1957) observed magnetic ordering of dilute Mn in 0.01 atomic percent Cu.

[39] M. A. Ruderman and C. Kittel, Phys. Rev. **96**, 99 (1954); T. Kasuya, Prog. Theor. Phys. **16**, 45 (1956).

[40] V. L. Ginzburg, Usp. Fiz. Nauk **101**, 185 (1970) [Sov. Phys. Usp. **13**, 335 (1970)].

[41] V. L. Ginzburg, Zh. Eksp. Teor. Fiz. **31**, 202 (1956) [Sov. Phys. JETP **4**, 153 (1957)].

[42] H. A. Blackstead and J. D. Dow, Phys. Rev. B **57**, 10 798 (1998).

[43] A. A. Abrikosov and L. P. Gor'kov, Zh. Eksp. Teor. Fiz. **39**, 1781 (1960) [Sov. Phys. JETP **12**, 1243 (1961)].